INTERNATIONAL JOURNAL FOR NUMERICAL METHODS IN FLUIDS, VOL. 12, 383–400 (1991)

# NUMERICAL SOLUTIONS FOR IMPULSIVELY STARTED AND DECELERATED VISCOUS FLOW PAST A CIRCULAR CYLINDER

XUEGENG WANG AND CHARLES DALTON

*Department of Mechanical Engineering, University of Houston, Houston, TX 77204-4814, U.S.A.*

## SUMMARY

A finite difference study of the unsteady two-dimensional flow past a circular cylinder has been conducted using vorticity and streamfunction as the dependent variables. The two cases considered were impulsively started and decelerated flows. The impulsively started problem was considered to validate the method and has yielded results which agree quite closely with existing results from both calculations and experiments. The decelerated flow analysis produced results which can be explained in terms of induced velocity effects from existing wake vortices for both suddenly stopped and uniformly decelerated flows.

KEY WORDS Circular cylinder Impulsively started flow Decelerating flow Finite difference solution Vortex shedding Drag and lift coefficients

## INTRODUCTION

The impulsively started flow of a viscous incompressible fluid past a stationary circular cylinder has been the subject of a number of numerical studies. For the purposes of this study we will define an impulsive start in the mathematical sense as opposed to the physical sense. Previous investigations have typically taken two different approaches to the cylinder problem. The first is a purely viscous flow numerical solution while the second is either a direct numerical simulation or a turbulence model solution or a combination of both.

Most of the viscous flow studies have dealt with the short-time or low-Reynolds-number ($Re$) cases, the implication being that the wake remains symmetric and that no turbulence is present in the flow field. The symmetric wake case has been studied in References 1–8. There have been several computational studies in which the wake was allowed to become asymmetric with the attendant alternate and periodic shedding of vortices. For a purely viscous flow, these asymmetric wake studies are also limited in both time and Reynolds number, but the upper bounds on each for physical reality are larger than for the symmetric wake case. The asymmetric wake case, with vortex shedding, has been studied in References 2, 3, 5 and 9–12.

Calculations for flows in which turbulence is present have been fewer and more recent than the purely viscous flow solutions. Tamura *et al.*,[13] Tsuboi *et al.*[14] and Braza and Ha Minh[15] have been the most visible among several in calculating high-Reynolds-number flows by means of a direct numerical simulation of the two-dimensional Navier–Stokes equations. Tamura *et al.* calculated drag coefficients of about 1·7 at $Re = 3000$ and about 1·8 at $Re = 10\,000$. Both of these values are about 50% higher than the experimentally determined values for flow past a rigid

0271–2091/91/040383–18$09.00

*Received 16 June 1989*
*Revised 25 April 1990*

circular cylinder. In a continuing study by the same authors, Tsuboi *et al.* calculated drag coefficients of about 1·7 at $Re = 10^5$ and about 0·8 at $Re = 6 \times 10^5$. These values are also about 50% high. Braza and Ha Minh calculated drag coefficients and Strouhal numbers which agree very well with data at both $Re = 3000$ and 10 000. Turbulence models have recently been used by Holmes and Connell[16] and Song and Wang.[17] Holmes and Connell used the $k$–$\varepsilon$ model and an adaptive grid scheme to calculate the flow past a cylinder at $Re = 40$ and 4000. They calculated a Strouhal number of 0·17, which compares well with the experimental value of 0·18 at $Re = 4000$. However, they computed no other parameters which could be compared to experimental values. Song and Wang used an eddy viscosity model to calculate a cylinder flow at a Reynolds number of $1{\cdot}4 \times 10^5$. The drag coefficient calculated by Song and Wang was about 25% too high while the lift coefficient was about 40% too high. Even though each of these high-$Re$ studies involved the calculation of other parameters, it is sufficient to cite only drag and lift coefficient values to see that high-$Re$ flows are not fully understood computationally.

These direct numerical simulations and turbulence models offer considerable hope for cylinder flow calculations at Reynolds numbers for which turbulence is present, but, except for the results of Braza and Ha Minh, there still appears to be room for progress in obtaining more accurate solutions. However, it is not the intention of this study to report the computation of flows when turbulence is present. Our approach will deal only with purely viscous flows.

An aspect of unsteady flow about a circular cylinder which apparently has escaped attention in numerical studies is a decelerated flow. In this study we examine situations consisting of a suddenly stopped flow and a uniformly decelerating flow. In the suddenly stopped flow case, which could be represented by the sudden closing of a butterfly valve, the cylinder is exposed to a rapidly decelerating fluid. Forces at least comparable to those in an impulsively started flow could be expected to act on the cylinder. The calculation of the flow field, especially the interactions of the wake with the cylinder, would yield an understanding of the reaction of the cylinder to the changing flow field.

In this paper we report the results of a series of numerical calculations for both impulsively started and decelerated flows. The impulsively started flow is used only to validate the procedure. The decelerated flow results are original to this effort. The wake is allowed to become asymmetric but there remains an elapsed time constraint because of the co-ordinate transformation employed in the numerical solution. When the shed vortices travel far enough downstream, the mesh size becomes too large for an accurate solution to be calculated. We do not allow the calculation to continue to times large enough for the vortices to be influenced by either the far-field mesh size or the downstream boundary.

## ANALYSIS

We represent the impulsively started or decelerated flow of a viscous incompressible fluid past a stationary circular cylinder as a two-dimensional flow with dominant viscous stresses. There are obvious Reynolds number limitations to these assumptions; these will be addressed as the results are presented. The governing equations are the vorticity transport equation,

$$\frac{\partial \omega}{\partial t} - \frac{1}{r}\left[\frac{\partial}{\partial r}\left(\omega \frac{\partial \psi}{\partial \theta}\right) - \frac{\partial}{\partial \theta}\left(\omega \frac{\partial \psi}{\partial r}\right)\right] = \nu \nabla^2 \omega, \tag{1}$$

and the equation relating the vorticity to the streamfunction,

$$\nabla^2 \psi = \omega, \tag{2}$$

where

$$\nabla^2 = \frac{\partial^2}{\partial r^2} + \frac{1}{r}\frac{\partial}{\partial r} + \frac{1}{r^2}\frac{\partial^2}{\partial \theta^2}.$$

In equations (1) and (2), $\omega$ is the two-dimensional vorticity, $\psi$ is the two-dimensional streamfunction with $r, \theta$ as the polar co-ordinates, $t$ is time and $v$ is the kinematic viscosity. The fluid velocities are found from

$$u = -\frac{1}{r}\frac{\partial \psi}{\partial \theta} \quad \text{and} \quad v = \frac{\partial \psi}{\partial r}. \tag{3}$$

The boundary conditions on the cylinder surface are

$$\psi = \partial\psi/\partial r = 0 \quad \text{on } r = R. \tag{4}$$

The $\theta$-variation of the dependent variables is taken to be periodic, with the values at $\theta = 0$ and $2\pi$ being the same.

The downstream boundary condition for the impulsively started cylinder is that the flow remains uniform at $r = \infty$. The actual downstream distance at which the infinity condition is applied depends on the Reynolds number, the elapsed time in the calculation and the parameter $a$ in the co-ordinate transformation to be applied. (The parameter $a$ will be defined in equation (5).) For example, when either the Reynolds number or the elapsed time is small, resulting in a symmetric wake, the infinity condition can be taken closer to the cylinder than for the case when vortex shedding occurs.

Since the major velocity gradients in the flow appear near the cylinder surface, it is necessary to find a co-ordinate transformation which will concentrate the mesh spacing near the surface. This is accomplished by setting

$$r = Re^{a\xi} \quad \text{and} \quad \theta = a\eta. \tag{5}$$

where $a$ is the transformation parameter, which is set equal to $\pi$ for this study, and $\xi$ and $\eta$ are the transformed variables. Figure 1 shows the system which would lead to $\Delta\xi = \Delta\eta$. We now define $\tau = U_\infty t/R$, $Re = 2U_\infty R/v$, $\tilde{\psi} = \psi/U_\infty R$, $\tilde{\omega} = \omega R/U_\infty$, $\tilde{u} = u/U_\infty$ and $\tilde{v} = v/U_\infty$. Equations (1) and (2) become

$$g(\xi)\frac{\partial \tilde{\omega}}{\partial \tau} - \frac{\partial}{\partial \xi}\left(\frac{\partial \tilde{\psi}}{\partial \eta}\tilde{\omega}\right) + \frac{\partial}{\partial \eta}\left(\frac{\partial \tilde{\psi}}{\partial \xi}\tilde{\omega}\right) = \frac{2}{Re}\nabla^2\tilde{\omega} \tag{6}$$

and

$$\nabla^2\tilde{\psi} = g(\xi)\tilde{\omega}, \tag{7}$$

with

$$\nabla^2 = \frac{\partial^2}{\partial \xi^2} + \frac{\partial^2}{\partial \eta^2} \quad \text{and} \quad g(\xi) = a^2 e^{2a\xi}.$$

The velocities are given by

$$\tilde{u} = U/\sqrt{[g(\xi)]} \quad \text{and} \quad \tilde{v} = V/\sqrt{[g(\xi)]}, \tag{8}$$

where

$$U = -\partial\tilde{\psi}/\partial\eta \quad \text{and} \quad V = \partial\tilde{\psi}/\partial\xi.$$

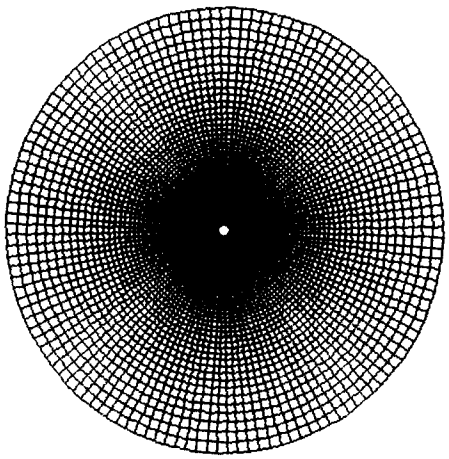

Figure 1. Coordinate system leading to $\Delta\xi = \Delta\eta$

The boundary conditions are now given by

$$\tilde{\psi} = \partial\tilde{\psi}/\partial\xi = 0 \quad \text{on} \quad \xi = 0 \tag{9}$$

and

$$\tilde{\psi} = 2\sinh(a\xi_\infty)\sin(a\eta) \quad \text{and} \quad \tilde{\omega} = 0 \quad \text{at} \quad \xi = \xi_\infty. \tag{10}$$

This now completes the system of governing equations and boundary conditions. Hereafter we will omit the tilde above the dimensionless variables and understand that we are working with dimensionless quantities.

## NUMERICAL SOLUTION

Equation (6) will be solved by a predictor–corrector finite difference scheme while equation (7) will be solved by an IMSL subroutine, a fast Poisson solver, based on a method known as the HODIE (high-order difference approximation with identity expansion) method as developed by Lynch and Rice.[18] This procedure generates fast approximate solutions, using fast Fourier transforms and correct to sixth order, and is well suited to equations like equation (7). The co-ordinate system selected to represent the problem provides for the use of the fast Poisson solver. There are variations of this co-ordinate transformation which have been used for the symmetric wake problem[1–5,7] and for the asymmetric wake problem.[2,3,11,12]

In finite difference form, equation (6) becomes

$$g(\xi)\frac{\partial\omega_{i,j}}{\partial\tau} = -\left(\frac{U_{i,j+1}\omega_{i,j+1} - U_{i,j-1}\omega_{i,j-1}}{2\Delta\xi}\right) - \left(\frac{V_{i+1,j}\omega_{i+1,j} - V_{i-1,j}\omega_{i-1,j}}{2\Delta\eta}\right)$$
$$+ \frac{2}{Re}\left(\frac{\omega_{i,j+1} - 2\omega_{i,j} + \omega_{i,j-1}}{\Delta\xi^2} + \frac{\omega_{i+1,j} - 2\omega_{i,j} + \omega_{i-1,j}}{\Delta\eta^2}\right), \tag{11}$$

where the subscript $i, j$ represents the mesh point $i, j$ in the co-ordinates $\eta, \xi$ respectively and the truncation error is $O(\Delta\xi^2, \Delta\eta^2)$. We set

$$U_{i,j} = -(\psi_{i+1,j} - \psi_{i-1,j})/2\Delta\eta \quad \text{and} \quad V_{i,j} = (\psi_{i,j+1} - \psi_{i,j-1})/2\Delta\xi. \tag{12}$$

Equation (11) is now written as

$$\partial \omega_{i,j}/\partial \tau = f_{i,j}, \tag{13}$$

where the right-hand side of equation (11) is divided by $g(\xi_j)$ and becomes $f_{i,j}$.

A two-step, three-level, finite difference, predictor–corrector scheme is used with the predictor based on the second-order Adams–Bashforth method,

$$\omega^*_{i,j} = \omega^n_{i,j} + (\Delta\tau/2)(3f^n_{i,j} - f^{n-1}_{i,j}), \tag{14}$$

where $n$ indicates the $n$th time step and the asterisk refers to the predicted value of $\omega$ (or $f$, $U$, $V$) at the $(n+1)$ time step. The corrector equation is

$$\omega^{n+1}_{i,j} = \omega^n_{i,j} + (\Delta\tau/12)(5f^*_{i,j} + 8f^n_{i,j} - f^{n-1}_{i,j}). \tag{15}$$

Note that the calculation of $f^*$ involves not only $\omega^*$ but also $U^*$ and $V^*$. The corrector gives a third-order-accurate value for $\omega^{n+1}_{i,j}$. Since equations (14) and (15) require information at the $(n-1)$ time step, the forward Euler method is used to calculate the first time step,

$$\omega^*_{i,j} = \omega^1_{i,j} + \Delta\tau f^1_{i,j}. \tag{16}$$

The corrector is given by

$$\omega^2_{i,j} = \omega^1_{i,j} + (f^*_{i,j} + f^1_{i,j})\Delta\tau/2. \tag{17}$$

These two equations provide for second-order accuracy in time for the first time step.

The initial conditions for the impulsive start problem are

$$u = \omega = \psi = 0 \quad \text{at } t = 0 \tag{18}$$

and

$$U = 1 \quad \text{at } t = \Delta t \text{ in the undisturbed flow.} \tag{19}$$

The solution procedure consists of the following steps.

1. The initial $\psi$-solution is the inviscid solution, i.e., the solution of the homogeneous form of equation (7).
2. Calculate a zero-time-step value of wall vorticity from

$$\omega_{i,1} = \frac{3\psi_{i,2}}{g_1 \Delta\xi^2} - \frac{g_2 \omega_{i,2}}{2g_1} + O(\Delta\xi)^2,$$

   in which $\omega_{i,2} = 0$ before the first time step. This equation is a second-order-correct extrapolation of the vorticity to the cylinder wall.
3. Solve equations (16) and (17) to obtain the vorticity after the first time step.
4. Solve equation (7) for $\psi$ using the vorticity field calculated in step 3. Determine a new wall vorticity from the equation in step 2 with $\omega_{i,2}$ not now necessarily equal to zero.
5. Solve equations (14) and (15) for the vorticity at the next time step.
6. Solve equation (7) for $\psi$ using the vorticity field calculated in step 5. Determine a new wall vorticity from the equation in step 2 with $\omega_{i,2}$ not now necessarily equal to zero.
7. Repeat steps 5 and 6.

A von Neumann linear stability analysis was performed for equations (11)–(15). The vorticity $\omega^n_{ij}$ was expanded in a Fourier series as

$$\omega^n_{ij} = \sum_k \sum_l A^n_{kl} \exp(2\pi k \hat{i} \xi_j) \exp(2\pi l \hat{i} \eta_i) \tag{20}$$

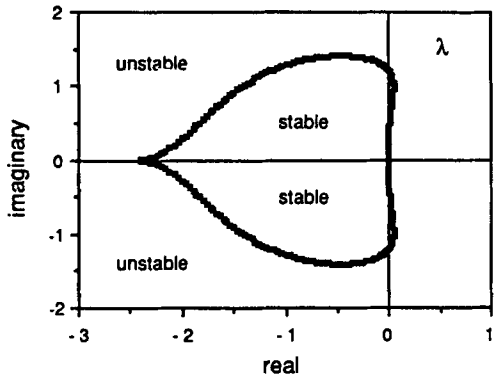


Figure 2. Stability of the present numerical scheme in terms of $\lambda$

and substituted into equation (11). The stability of the scheme requires that the Fourier modes do not increase with time, i.e., $|A_{kl}^{n+1}|<|A_{kl}^{n}|$. This yields

$$|(1+\tfrac{13}{12}\lambda_{kl}+\tfrac{5}{8}\lambda_{kl}^2)\pm\sqrt{[(1+\tfrac{13}{12}\lambda_{kl}+\tfrac{5}{8}\lambda_{kl}^2)-(\tfrac{5}{6}\lambda_{kl}^2+\tfrac{1}{3}\lambda_{kl})]}|<2, \tag{21}$$

where

$$\lambda_{kl}=\frac{\Delta\tau}{g(\xi_j)}\left[-U_{ij}\frac{\hat{\imath}\sin(2\pi k\Delta\xi)}{\Delta\xi}-V_{ij}\frac{\hat{\imath}\sin(2\pi l\Delta\eta)}{\Delta\eta}-\frac{4}{Re}\left(\frac{1-\cos(2\pi k\Delta\xi)}{(\Delta\xi)^2}\right)+\frac{1-\cos(2\pi l\Delta\eta)}{(\Delta\eta)^2}\right] \tag{22}$$

and $\hat{\imath}=\sqrt{(-1)}$.

Figure 2 shows the stable region of this flow; $\lambda_{kl}$ must be chosen so that its value is from the region labelled 'stable'. Equations (21) and (22) can be simplified by letting $\Delta\xi=\Delta\eta$. This substitution gives

$$\lambda=-\hat{\imath}\left[\frac{\Delta\tau u_{ij}}{\Delta\tilde{r}}\sin\left(\frac{2\pi k\Delta\tilde{r}}{a\tilde{r}_j}\right)+\frac{\Delta\tau v_{ij}}{\Delta\tilde{r}}\sin\left(\frac{2\pi l\Delta\tilde{r}}{a\tilde{r}_j}\right)\right]$$
$$-\frac{4\Delta\tau}{Re(\Delta\tilde{r})^2}\left[2-\cos\left(\frac{2\pi k\Delta\tilde{r}}{a\tilde{r}_j}\right)-\cos\left(\frac{2\pi l\Delta\tilde{r}}{a\tilde{r}_j}\right)\right], \tag{23}$$

where $\lambda$ is the same as in equation (22) except that $\lambda_{kl}$ has had the subscripts omitted, $a=\pi$ and $\tilde{r}$ is defined by $\tilde{r}=r/R$. The mesh size and time steps used herein provide for a conditionally stable solution.

## RESULTS FOR IMPULSIVELY STARTED AND DECELERATED FLOWS

### *Impulsive start*

The calculation procedure was verified for the impulsively started flow past a circular cylinder. Calculations have been performed for both symmetric and asymmetric wakes for several Reynolds numbers and comparison has been made with both flow visualization results and other calculations to demonstrate the correctness of the results.

Four different mesh sizes were examined to determine the appropriate mesh size for a physically correct solution at $Re=550$. The mesh sizes used were $\Delta\xi=\Delta\eta=1/32, 1/50, 1/64$

and 1/100. The solutions at 1/64 and 1/100 were the same and, as our discussion will show, yielded remarkably good comparison with flow visualization and other computational results. The results from calculations for 1/50 and 1/32 showed increasingly distinct differences from the 1/64 results. Three different time steps (0·02, 0·01 and 0·005) were used; the results were indistinguishable for a mesh spacing of 1/64. Thus the results presented herein are exclusively for a constant mesh spacing of $\Delta\xi = \Delta\eta = 1/64$ and a time step of $\Delta\tau = 0{\cdot}02$. These values are compatible with equation (23).

For an impulsively started flow at $Re \leqslant 40$, the physical wake is expected to remain symmetric for large times even if the flow is perturbed. For values of $Re > 40$ the physical wake will remain symmetric through some dimensionless time which depends on the value of $Re$ and then will become asymmetric with vortex shedding occurring.

Calculations have been performed at several Reynolds numbers at which other numerical solutions and flow visualization results exist. Ta Phuoc Loc[1] presented results of calculations at $Re = 300$, 550 and 1000, Chamberlain[6] presented results at $Re = 550$ and Braza *et al.*[9] at $Re = 1000$, all at times small enough for the physical wake to remain symmetric. The calculated results from the present study agree remarkably well with the cited results; the comparison includes both the streamfunction values and the wall vorticity distribution which is shown in Figure 3 at $Re = 550$. The wall vorticity shows clearly the features of the separated region, including the large and secondary wake vortices. Bouard and Coutanceau[19] also show flow visualization results at $Re = 300$ and 550. All of the calculated results previously mentioned and the present results show very good agreement with the flow visualization results of Bouard and Coutanceau. These comparisons are not shown here.

The numerical solutions produce symmetric wakes either at Reynolds numbers or elapsed times greater than those for which vortex shedding is expected to occur. Therefore it is necessary to perturb the flow calculation, $0 < \tau \leqslant 5$, to stimulate wake asymmetry and vortex shedding. This perturbation consisted of increasing the dimensionless $\psi$-value on the cylinder surface by 0·005. For $\tau > 5$ the perturbation was removed and the numerical solution progressed according to the procedure described in the analysis section. The results of a perturbed solution are shown in Figure 4 at $Re = 102$ and $\tau = 40$, with $\Delta\xi = \Delta\eta = 1/64$ and $\Delta\tau = 0{\cdot}02$. The streamfunction

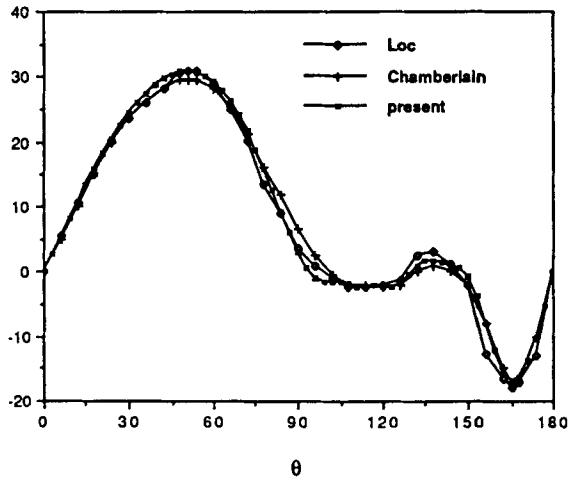


Figure 3. Wall vorticity for $Re = 550$, $\tau = 5{\cdot}0$ at $\Delta\xi = \Delta\eta = 1/64$, $\Delta\tau = 0{\cdot}02$

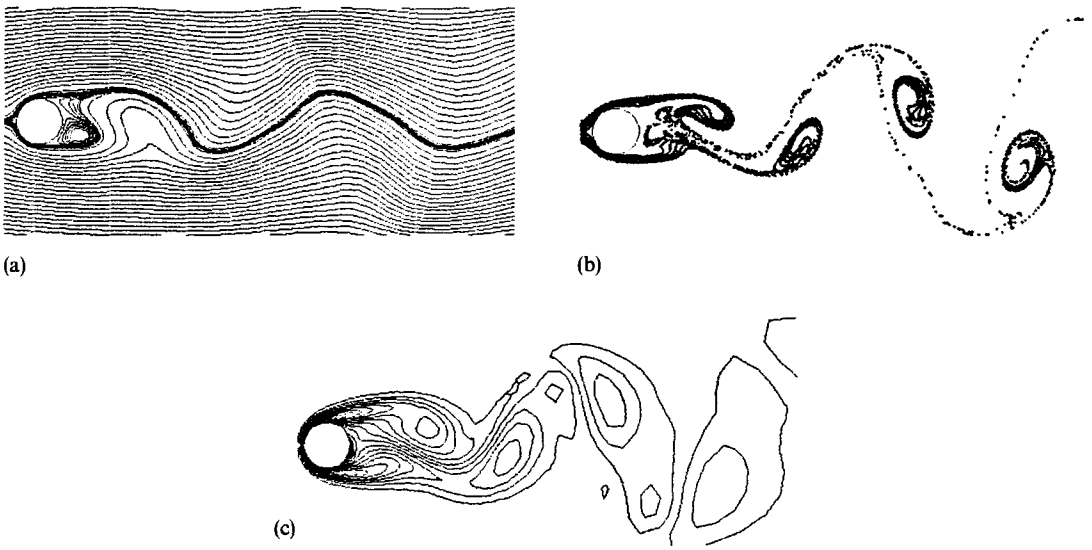


Figure 4. (a) $\psi$ plot, (b) streaklines, (c) $\omega$ plot, $Re = 102$, $\tau = 40$, $\Delta\xi = \Delta\eta = 1/64$, $\Delta\tau = 0{\cdot}02$

plot looks similar to the streamfunction plots of many other investigators of this problem. The results have the same streamfunction behaviour in the wake as observed by Dougherty *et al.*[12] and Fang.[11] However, comparison between flow visualization pictures and streamfunction calculations cannot be made directly since flow visualization patterns result from streaklines, not streamlines. Thus, to have more confidence in our results, we calculated the streaklines which would correspond to the calculated streamfunction distribution. The streakline calculation was done by following fluid elements which passed through a vertical array of points just upstream from the stagnation point. The array of points was arranged with five points just above and five points just below the dividing streamline. The streakline calculation was a first-order Lagrangian process and these results are also shown in Figure 4. The streakline calculation produces a flow field remarkably like that of Taneda as depicted in van Dyke's book[20] at a Reynolds number of 105.

The drag and lift coefficients for this example at $Re = 102$ are shown in Figure 5. The asymptotic value of $C_D$ for large time agrees quite well with the experimental value. The lift coefficient was found to oscillate at the correct frequency (the Strouhal frequency) and the drag coefficient exhibits the expected small-amplitude oscillations at twice the Strouhal frequency. Calculations were also made at $Re$-values of 140 and 200 and showed equally good comparison with experimental results. These results are shown in Figure 6.

*Decelerated flow*

The decelerated flow calculations are done for four different situations. In the first two cases the mathematical simplification of an instantly stopped flow is applied. The first situation to be presented is for the initial condition (short-time solution for the impulsive start) of a symmetric wake while the second situation has an unsymmetric wake (long-time solution for the impulsive start) for the initial condition, both for a suddenly stopped flow. In the last two cases a uniform deceleration of the flow is applied. The third of the four situations examines the flow when the

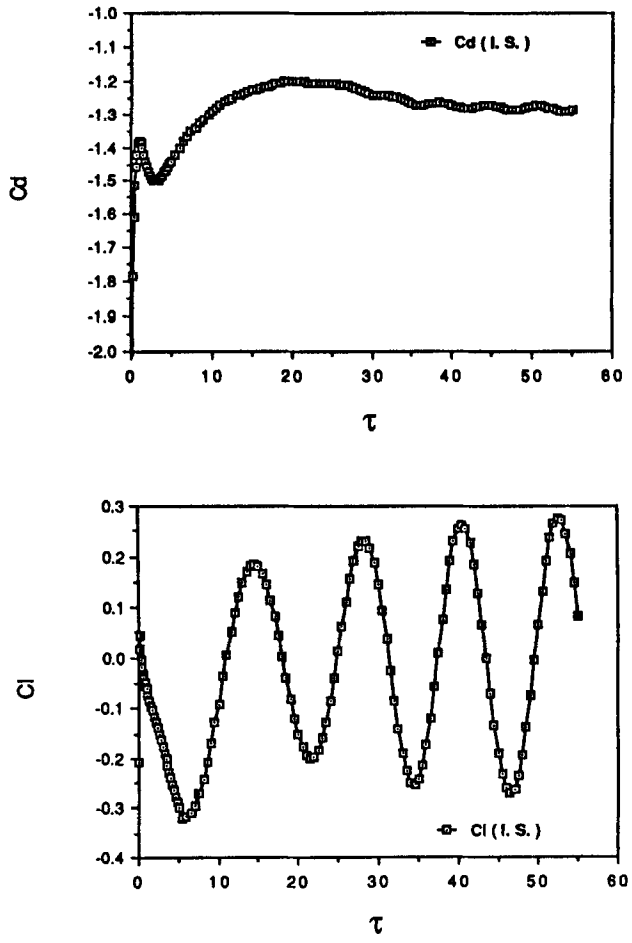


Figure 5. Drag and lift coefficients for Figure 4 example

deceleration occurs when the original wake is symmetric. The fourth is when the deceleration occurs for an original wake which is unsymmetric. In all cases the velocity in the drag coefficient definition is the initial velocity before deceleration begins.

The case of $Re = 550$ with a symmetric wake was also studied by Ta Phuoc Loc[1] and Chamberlain[6] and the wall vorticity comparison is shown in Figure 3 as mentioned earlier. The agreement is excellent; the wake vortices are clearly shown. The impulsive start solution at $\tau = 5$ represents the initial condition for the sudden stop calculation. The drag coefficient at the first time step for the impulsive start was approximately 37, while the value for the sudden stop first time step was approximately 55, an increase of almost 50%. We recognize that the actual value of the drag coefficient is not meaningful at each of these first time steps; the values are mentioned to show the relative difference between them. The behaviour for both cases after several time steps is shown in Figure 7. The direction of the force acting on the cylinder is observed to reverse twice as time increases. The force reversal is explained by the wake vortex motion which is produced by

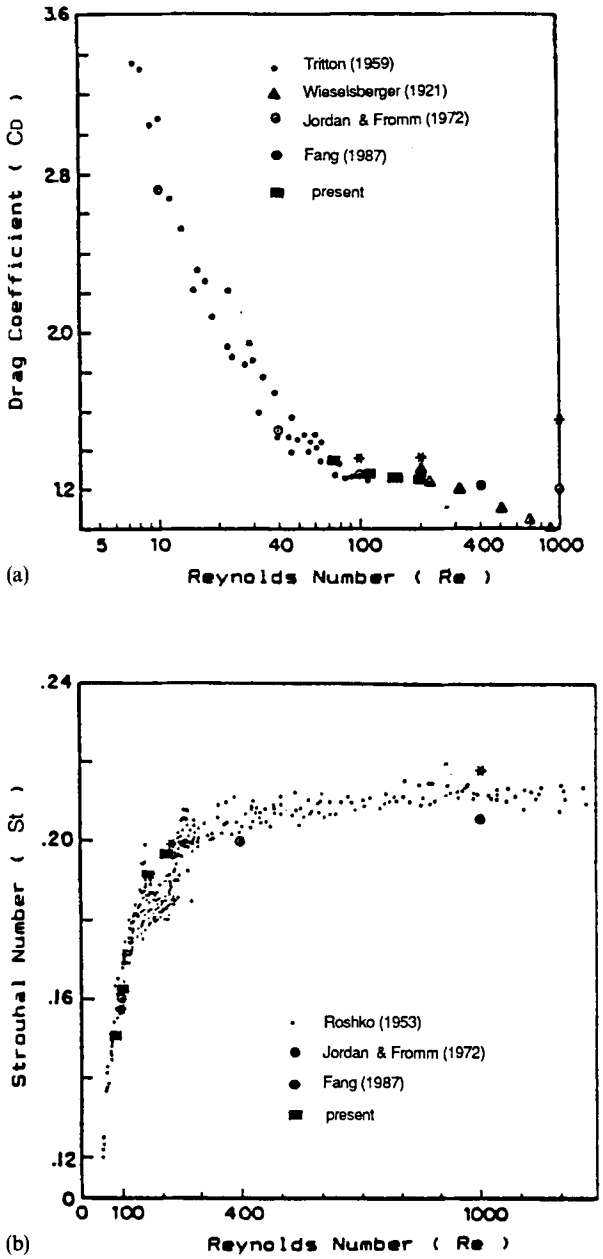


Figure 6. Comparison of numerical and experimental data: (a) drag coefficient vs. *Re*; (b) Strouhal number vs. *Re*. (See References 22–25)

the velocity each vortex induces on the other. The solution is shown in Figure 8 at $\tau = 7$. The instant the flow is stopped, a strong inertial force is generated in the opposite direction to the drag force developed by the impulsive start flow. This inertial force decreases rapidly and, over less than one dimensionless time unit, is again in the direction of the original drag force. The force

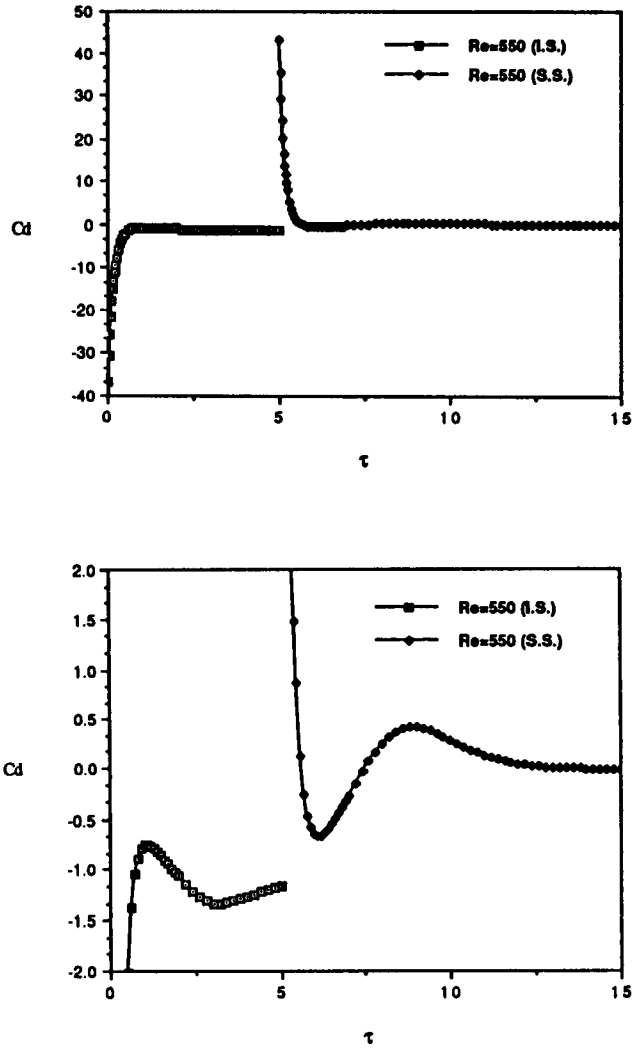


Figure 7. Drag coefficient for impulsive start and sudden stop case at $Re = 550$

continues to increase as the vortices move towards the cylinder. The force increase is diminished as a new pair of vortices is formed at the cylinder shoulders. The force then asymptotically approaches zero as the vortices diffuse and the effects of the sudden stop vanish. All of this is seen clearly in Figure 8.

The second case for the suddenly stopped flow is with an initial condition given by the impulsive start solution shown in Figure 4 at $Re = 102$ and $\tau = 40$. For this case, because of vortex shedding, there will be a time-dependent lift variation as well as drag. This is shown in Figure 9. Again we note the sharp change in magnitude and direction of the drag force as the flow is suddenly stopped. Although it is not as evident as for the symmetric wake case owing to the ordinate scale in Figure 9, the drag experiences the same behaviour as for the example depicted in

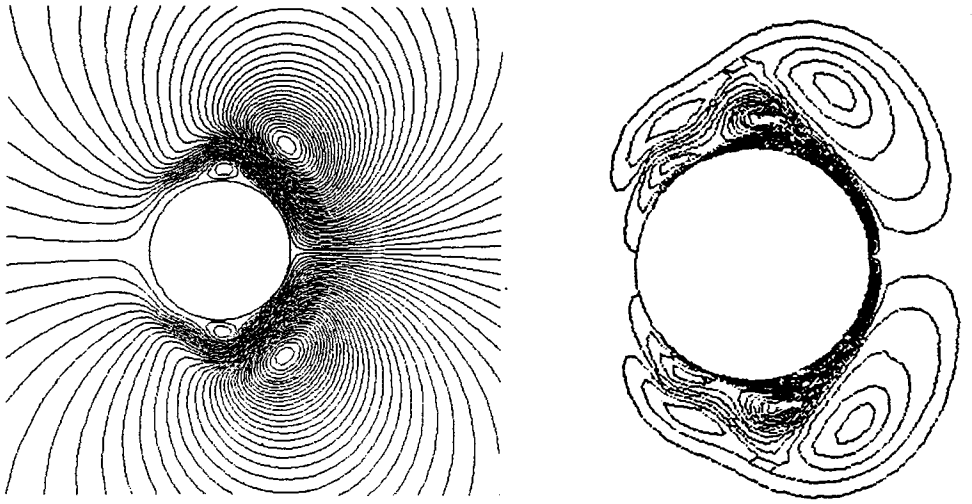

(a) (b)

Figure 8. (a) $\psi$ plot, (b) $\omega$ plot; for $Re = 550$, $\tau = 7$

Figure 7. The lift coefficient reverses sign twice as the asymmetric near wake passes over the cylinder. The streaklines are shown in Figure 10 at $\tau = 55$; the solution is actually carried out to $\tau = 80$ but is not shown herein. The far-wake vortices do not have appreciable motion during this time interval and the lift appears to be converging towards zero. However, as the nearest-wake vortex approaches the cylinder, the lift will begin to be affected again.

When the flow is uniformly decelerated from a constant velocity to zero, the forces do not change as dramatically as in the suddenly stopped flow. However, there are still many interesting flow phenomena present, which have been observed by means of flow visualization by Tatsuno and Taneda.[21] Two cases have been calculated in the present study in order to make direct comparisons with the Tatsuno and Taneda flow visualization results, which did not include any force measurements. The flow is first impulsively started and the wake is allowed to become fully developed and then the flow starts to decelerate. In the first case the Reynolds number is $Re = 36{\cdot}5$ and the dimensionless deceleration parameter is $a'D^3/\nu^3 = 139$, where $a'$ is the deceleration of the flow. The computational parameters are the following: mesh sizes $\Delta\xi = \Delta\eta = 1/64$, mesh system $65 \times 129$, time step $\Delta\tau = 0{\cdot}01$ and outside boundary $\xi_\infty = 1{\cdot}0$ ($r_\infty = 23R$). The calculated wake development is shown in Figure 11 from $\tau = 10{\cdot}00$ to $27{\cdot}25$. From this figure we can see that as the incident flow decelerates, the influence of the wake vortices becomes increasingly stronger and the wake shape starts to grow and become bigger and bigger. The length of the wake is plotted in Figure 12 as a function of dimensionless time $a't/U$, as was originally used by Tatsuno and Taneda. Small deviations are observed between the calculated results and the experimental data as the flow decelerates. This deviation can be explained by the measurement of the wake length. Unlike the numerical simulation, zero streamlines which divide the separation bubbles from the main flow can hardly be identified from a flow visualization picture. Despite these small deviations, the comparison is still fairly good.

The second case of the uniformly decelerating flow problem is solved for $Re = 77$ and $a'D^3/\nu^2 = 105$, with mesh sizes $\Delta\xi = \Delta\eta = 1/64$, mesh system $81 \times 129$, time step $\Delta\tau = 0{\cdot}01$ and

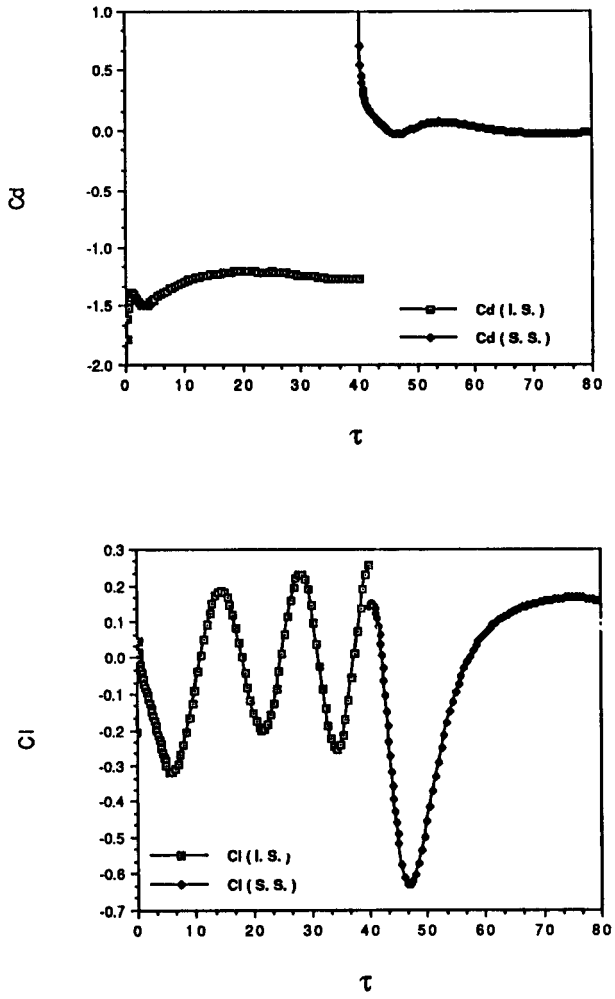


Figure 9. Drag and lift coefficients for the sudden-stop case at $Re = 102$, $\Delta\xi = \Delta\eta = 1/64$, $\Delta\tau = 0{\cdot}02$

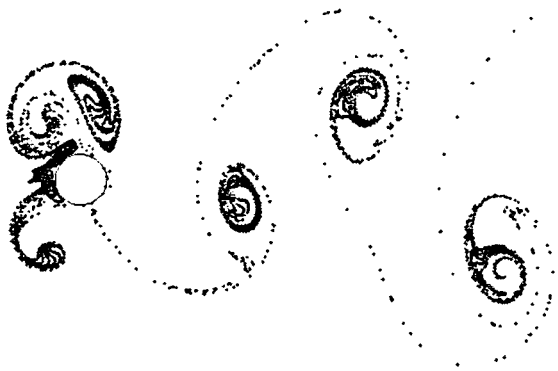

Figure 10. Streakline plot for the sudden-stop case for $Re = 102$ at $\tau = 55$

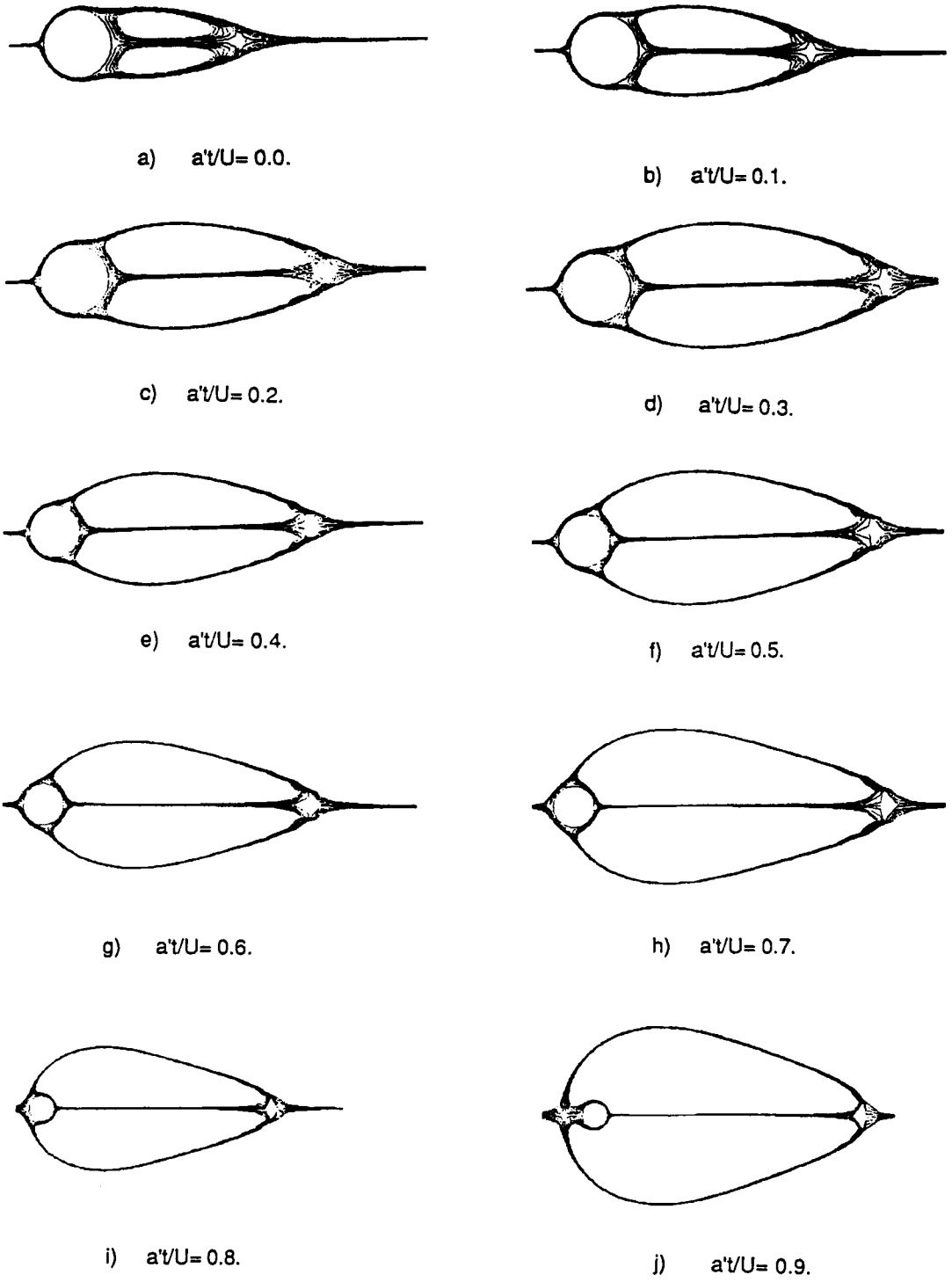


Figure 11. Calculated wake change for a uniformly decelerating flow with $a'D^3/\nu^2 = 139$ and an initial Reynolds number of 36·5

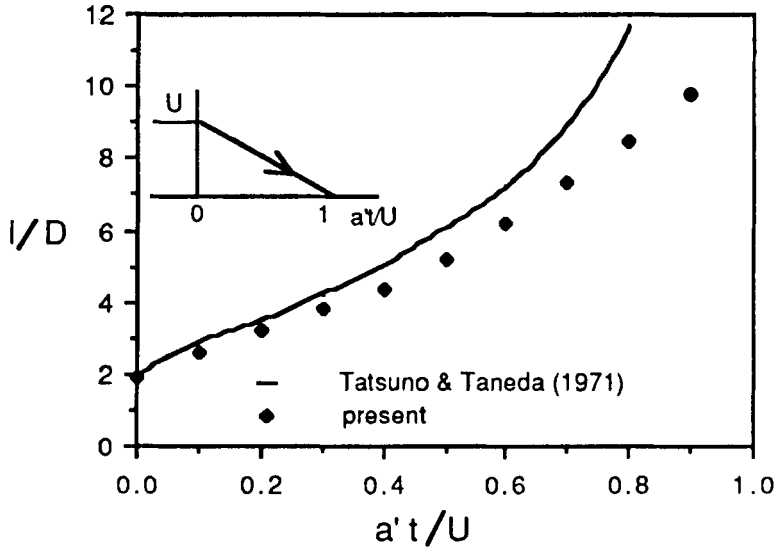


Figure 12. Wake-length change for the conditions of Figure 11

outside boundary $\xi_\infty = 1{\cdot}25$ ($r_\infty = 51R$). The flow calculation is perturbed to generate an asymmetric wake. Again the flow is impulsively started at $\tau = 0$ and the wake is allowed to develop to $\tau = 40$ and then flow deceleration starts. The flow patterns in the deceleration process are shown in Figure 13 from $\tau = 40$ to 165·94. The flow visualization by Tatsuno and Taneda,[21] who did not publish any force measurements for this case either, are also shown in Figure 13(c) at $\tau = 140{\cdot}78$ and in Figure 13(d) at $\tau = 165{\cdot}94$. The calculated results agree very well with the flow visualization results. The time variations of the drag and lift coefficients are shown in Figure 14. Since the deceleration of the flow is very slow, the incident flow dominates the motion of the wake vortices for a fairly long dimensionless time before the wake vortices start to move back and interact with the cylinder. During this time period, the strength of the wake vortices becomes weaker and weaker due to viscous diffusion. Thus, when they finally encounter the cylinder as they move back, no significant force change is observed. However, the lift force changes its sign as the wake vortices with different circulations move back and interact with the cylinder. The sudden change in drag coefficient which occurs at $\tau = 152{\cdot}10$ is because of the discontinuity in the deceleration at this time.

## CONCLUSIONS

The finite difference calculations undertaken herein have been tested for the benchmark case of an impulsively started viscous flow. A predictor–corrector method for the vorticity transport equation was used along with a fast Poisson solver for the streamfunction equation. Very good comparison with experimental data and other calculations has been found for the test case. The proven calculation procedure was then applied to the suddenly stopped and uniformly decelerated flow problems. A sharp increase in drag coefficient over that for the impulsive start was found when the initial condition wake vortices were symmetric for the suddenly stopped flow case. When the initial condition wake was asymmetric, the increase in drag coefficient was not so

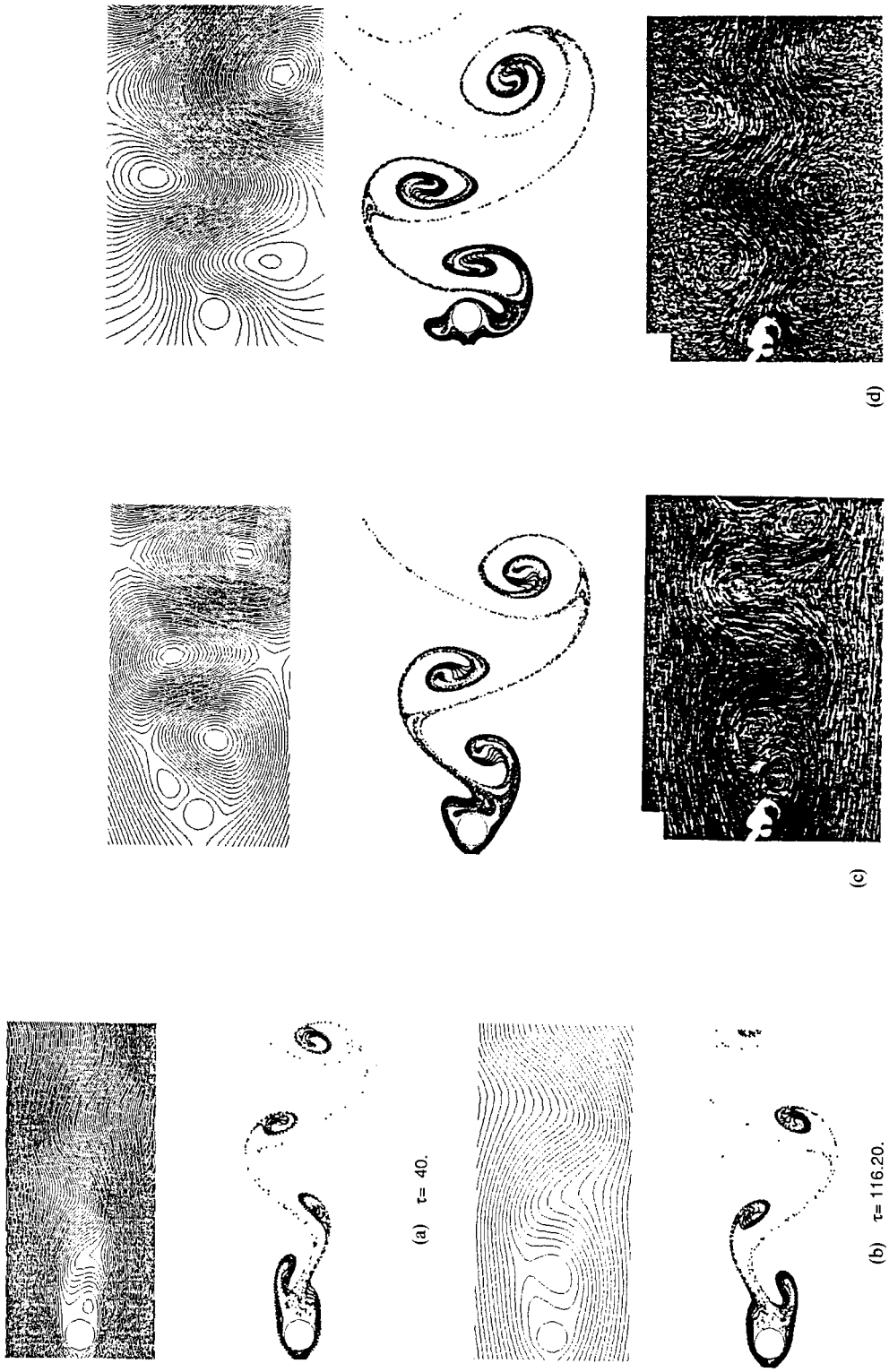


Figure 13. Calculated wakes and flow-visualization results for a uniformly decelerating flow with $a'D^3/\nu = 105$ and an initial Reynolds number of 77

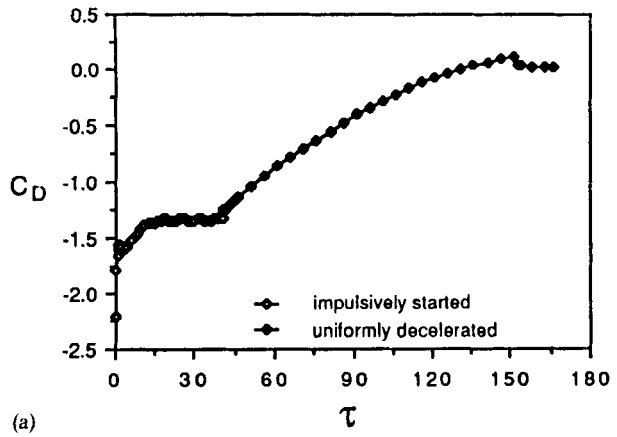


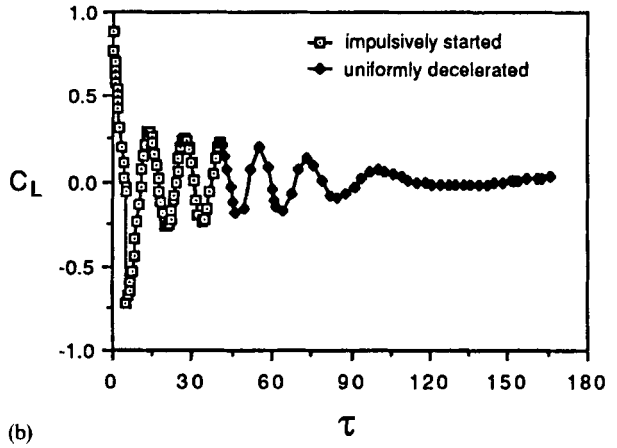


Figure 14. Uniformly decelerating flow, $Re = 77$, $a'D^3/\nu^2 = 105$. (a) drag coefficient; (b) lift coefficient

dramatic and an initial increase in lift coefficient was observed. These changes in lift and drag on the cylinder can be explained in terms of the induced velocities generated by the initial condition wake vortices.

ACKNOWLEDGEMENTS

We thank Pineridge Press for its approval to use Figure 6 and the *Journal of the Physical Society of Japan* for its approval to use Figures 13(c) and 13(d). A shorter version of this paper was presented at the International Conference on Numerical Methods in Laminar and Turbulent Flow in Swansea, U.K. in July 1989 and was published in the Conference Proceedings by Pineridge Press.

## REFERENCES


1. Ta Phuoc Loc, 'Numerical analysis of unsteady secondary vortices generated by an impulsively started circular cylinder', *J. Fluid Mech.*, **100**, 111–128 (1980).
2. Y. Lecointe and J. Piquet, 'On the use of several compact methods for the study of unsteady incompressible viscous flow round a circular cylinder', *Comput. Fluids*, **12**, 255–280 (1984).
3. L. C. Chien and Y. P. Wang, 'Numerical solution for separated flow around an impulsively started circular cylinder', *Numerical Methods in Laminar and Turbulent Flow*, Pineridge Press, Swansea, 1985, pp. 609–620.
4. Ta Phuoc Loc and R. Bouard, 'Numerical solution of the early stage of the unsteady viscous flow around a circular cylinder: a comparison with experimental visualization and measurements', *J. Fluid Mech.*, **160**, 93–117 (1985).
5. A. Borthwick, 'Comparison between two finite-difference schemes for computing the flow around a cylinder', *Int. j. numer. methods fluids*, **6**, 275–290 (1986).
6. R. R. Chamberlain, 'Unsteady flow phenomena in the near wake of a circular cylinder', *AIAA Paper 87-0371*, Reno, NV, 1987.
7. C. L. Rumsey, 'Details of the computed flowfield over a circular cylinder at Reynolds number 1200', *J. Fluids Eng.*, **110**, 446–452 (1988).
8. C. R. Anderson, 'Vorticity boundary conditions and boundary vorticity generation for two-dimensional viscous incompressible flows', *J. Comput. Phys.*, **80**, 72–97 (1988).
9. M. Braza, P. Chassaing and H. Ha Minh, 'Numerical study and physical analysis of the pressure and velocity fields in the near wake of a circular cylinder', *J. Fluid Mech.*, **165**, 79–130 (1986).
10. B. E. Eaton, 'Analysis of laminar vortex shedding behind a circular cylinder by computer-aided flow visualization', *J. Fluid Mech.*, **180**, 117–145 (1987).
11. J. Fang, 'Numerical simulation of unsteady incompressible flow past a circular cylinder', *M.S. Thesis*, University of Alabama, Huntsville, AL, 1987 (unpublished).
12. N. Dougherty, J. Holt, B. Liu and J. O'Farrell, 'Time-accurate Navier–Stokes computations of unsteady flows: the Karman vortex street', *AIAA Paper 89-0144*, Reno, NV, 1989.
13. T. Tamura, K. Tsuboi and K. Kuwahara, 'Numerical simulation of unsteady flow patterns around a vibrating cylinder', *AIAA Paper 88-0128*, Reno, NV, 1988.
14. K. Tsuboi, T. Tamura and K. Kuwahara, 'Numerical study for vortex induced vibration of a circular cylinder in high Reynolds number flow', *AIAA Paper 89-0294*, Reno, NV, 1989.
15. M. Braza and H. Ha Minh, 'Direct numerical simulation of certain 2-D transition features of the flow past a circular cylinder', *Proc. Eighth Int. Conf. on Offshore Mechanics and Arctic Engineering*, ASME, The Hague, 1989, pp. 401–410.
16. D. G. Holmes and S. D. Connell, 'Solution of the 2D Navier–Stokes equations on unstructured adaptive grids', *AIAA Paper 89-1932*, Buffalo, NY, 1989.
17. C. C. S. Song and M. Yuan, 'Simulation of vortex-shedding flow about a circular cylinder at high Reynolds numbers', *J. Fluids Eng.*, **112**, 155–163 (1990).
18. R. E. Lynch and J. R. Rice, 'High accuracy finite-difference approximations to solutions of elliptic partial differential equations', *Proc. Natl Acad. Sci. U.S.A.*, **75**, 2541–2544 (1978).
19. R. Bouard and M. Coutanceau, 'The early stage of development of the wake behind an impulsively started cylinder for $40 < Re < 10^4$', *J. Fluid Mech.*, **101**, 583–607 (1980).
20. M. van Dyke, *An Album of Fluid Motion*, Parabolic Press, Stanford, CA, 1982, p. 57.
21. M. Tatsuno and S. Taneda, 'Visualization of the unsteady flow past cylinders and plates decelerated from a steady speed', *J. Phys. Soc. Jpn.*, **31**, 1266–1274 (1971).
22. A. Roshko, 'On the development of turbulent wakes from vortex streets', *NACA Tech. Rep. 1191*, 1953.
23. D. J. Tritton, 'Experiments on the flow past a circular cylinder at low Reynolds numbers', *J. Fluid Mech.*, **6**, 547–567 (1959).
24. S. K. Jordan and J. E. Fromm, 'Oscillatory drag, lift, and torque on a circular cylinder in a uniform flow', *Phys. Fluids*, **15**, 371–380 (1972).
25. C. Wieselsberger, 'Nuere Feststellungen über die Gesetze des Flüssigkeits- und Luftwiderstands', *Phys. Z.*, **22**, 321–328 (1921).